DOI: 10.1002/ejic.201000575

Synthetic Routes and Plasmonic Properties of Noble Metal Nanoplates

Isabel Pastoriza-Santos,*[a] Ramón A. Alvarez-Puebla,[a] and Luis M. Liz-Marzán[a]

Keywords: Nanoplates / Gold / Silver / Plasmons / Synthesis design / SERS

This article provides an overview of recent research on the synthesis and surface-plasmon-related properties of noble metal nanoplates. The first part is dedicated to summarizing the most relevant wet-chemical and physical synthetic protocols that have been used to obtain Au and Ag nanotriangles/nanoplates in high yield, with a discussion of the formation mechanisms proposed by the different authors. Finally, we present a description of the characteristic optical properties of nanoparticles with this particular morphology, in relation with the possibility of exciting different surface plasmon modes and concentrating high electromagnetic fields at certain areas, which is important for applications in surface-enhanced Raman scattering (SERS).

Introduction

Nanosized metal particles are the building blocks of the emerging and highly promising field of plasmonics,[1] which deals with the collective excitations of conduction electrons, light amplification at the nanoscale,[2] and their potential applications in fields such as electronics,[3] catalysis,[4] optical sensing,[5] or nanobiomedicine.[6] Synthetic routes for the fabrication of plasmonic nanostructures with controlled shape, size, and composition have undergone a severe revolution over the last ten years. Regarding gold, it is possible nowadays to prepare almost any imaginable structure in high yield.[7] However, in the case of silver, although progress in the control of the possible sizes and geometries is not comparable to that for gold, the preparation of well-

[a] Departamento de Química Física and Unidad Asociada CSIC-Universidade de Vigo,
36310 Vigo, Spain
Fax: +34-986812556
E-mail: pastoriza@uvigo.es

Isabel Pastoriza-Santos is currently Assistant Professor in Physical Chemistry at the University of Vigo, at which she also received her BSc (1997) and PhD (2001) degrees. She also worked as a postdoc in the Chemistry School at the University of Melbourne with Prof. Paul Mulvaney during 2002–2003. Her current interests involve the synthesis, surface modification, and assembly of metal nanoparticles and the study of their characteristic optical properties.

Ramón A. Alvarez-Puebla is a Research Fellow at the Department of Physical Chemistry, University of Vigo. He worked as a postdoc in the Department of Chemistry of the University of Windsor (Canada) with Prof. Ricardo Aroca. He was appointed as Research Officer at the National Institute for Nanotechnology of the National Research Council of Canada. He has co-authored 60 articles and holds two patents. His current interests involve electronic and vibrational spectroscopy, surface-enhanced spectroscopy, and their application for sensor fabrication.

Luis M. Liz-Marzán received his PhD from the University of Santiago de Compostela in 1992. He worked as a postdoctoral fellow at the Van't Hoff Laboratory (Utrecht University) and as visiting professor at Tohoku University and the University of Michigan. He joined the University of Vigo in 1995, where he currently is a Full Professor. He has co-authored over 180 articles and three patents, is recipient of several research awards, editor and editorial advisory board member of several chemistry and materials science journals. His current interests include the synthesis and assembly of nanoparticles, nanophotonics, and the development of nanoparticle-based biosensors.

defined structures has also been achieved either directly through physical or chemical routes or after one or more purification steps.[8] In contrast, control over other plasmonic metals such as copper, palladium, platinum, ruthenium, rhodium, or even alkaline elements remains still marginal.

The optical properties of plasmonic nanoparticles are essentially determined by three factors: composition, size, and shape.[9] While the first two were understood a long time ago, the effect of shape has only recently been fully appreciated. Not only do the energies of localized surface plasmon resonances (LSPR) within a given particle strongly depend on its shape, but additionally the distribution of LSPRs in anisotropic particles is not homogenous but concentrated at specific surface sites. This has been theoretically and experimentally demonstrated for a variety of shapes such as decahedra,[10] plates,[11] rods,[12] stars,[13] and other nanoparticles with tips,[14] and it has paved the way toward the design of new, advanced optical sensors with capabilities of detecting analytes down to the zeptomol regime in periods of time shorter than 1 s. Conversely, and for most plasmonic applications, surface chemistry is a key factor, not mainly because it has a direct impact on the LSPR frequency of a given nanoparticle, but because direct contact between the target molecule and the noble metal surface is needed to obtain a plasmon-derived effect.[15] With these considerations in mind, together with the advantage of having structures that can be easily organized on flat substrates, with the possibility of tuning their plasmonic response from the visible through the infrared, nanoplates emerge as one of the principal alternatives for the design of plasmonic devices, in particular for advanced sensing.

In this microreview, we aim at surveying the most common physical and chemical methods for the preparation of colloidally stable and organized arrays of gold and silver nanoplates, their optical response toward incident electromagnetic radiation, and their application for the design of ultrasensitive sensors specially based on surface-enhanced Raman scattering (SERS) spectroscopy.[16]

Synthetic Routes for the Fabrication of Ag and Au Nano- and Microplates

During the last decade, a number of synthetic methods have been developed to fabricate Ag and Au nano- and microplates in high yield. This section focuses on reviewing the different approaches, classified in wet methods, including photoinduced and chemical reduction, and physical methods, such as nanosphere lithography.

Photoinduced Methods

Most of the reported photoinduced strategies were designed for the fabrication of Ag nanoparticles, probably except the recent report by Zhu et al.[17] Using 1-butyl-3-methylimidazolium tetrafluoroborate (an ionic liquid) as reaction medium, template and capping agent, the authors obtained Au microplates with sizes of the order of tens of micrometers by photochemical reduction of Au^{3+}. Focusing back on Ag, the first photoinduced method was published by Jin et al.[18] Irradiation of preformed tiny Ag seeds (stabilized by citrate) with visible light, in the presence of bis(*p*-sulfonatophenyl)phenylphosphane dihydrate dipotassium salt (BSPP), induced their conversion into Ag nanoprisms with 100 nm edge length. The authors proposed a mechanism based on the initial formation of small silver nanoprisms and clusters from the preformed seeds and subsequent growth of the nanoprisms at the expense of the small clusters. In a later work, the same authors reported the ability to tune particle size (from 30 nm to 120 nm edge length) by adjusting the illumination wavelength. Longer wavelengths produced larger particles and, by employing dual-beam illumination (Figure 1), unimodal (rather than bimodal) growth of the nanoparticles was possible.[19] Indeed, they observed a bimodal nanoprism size distribution when the preformed seeds were irradiated with a single laser beam, whereas by using a so-called secondary beam, the fusion of preformed nanoprisms was avoided, as well as the formation of a second population of larger particles, thereby facilitating the slow growth of the smaller nanoprisms by the primary beam. However, it has been recently reported that monodisperse silver nanoprisms could be obtained through single-beam excitation by simply adjusting the solution pH,[20] which seems to be related to the influence of surface charge on the fusion between nanoprisms. Almost simultaneously, Junior et al.[21] and Sun and Xia.[22]

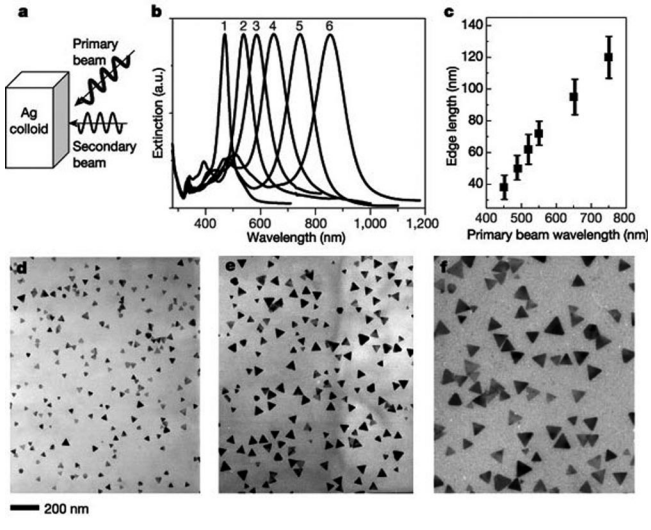

Figure 1. The unimodal growth of nanoprisms. (a) Schematic diagram of dual-beam excitation. (b) Optical spectra (normalized) for six different-sized nanoprisms [edge lengths: 38 ± 7 nm (1), 50 ± 7 nm (2), 62 ± 9 nm (3), 72 ± 8 nm (4), 95 ± 11 nm (5), and 120 ± 14 nm (6)] prepared by varying the primary excitation wavelength (central wavelength at 450, 490, 520, 550, 650, and 750 nm, respectively; width: 40 nm) coupled with a secondary wavelength (340 nm; width: 10 nm). (c) Edge lengths as a function of the primary excitation wavelength. (d–f) TEM images of Ag nanoprisms with average edge lengths of 38 ± 7 nm (d), 72 ± 8 nm (e), and 120 ± 14 nm (f). The scale bar applies to panels d–f. Reproduced with permission from ref.[29]

demonstrated that Ag nanoprisms were also formed when poly(vinylpyrrolidone) (PVP) was used instead of BSPP, thus generalizing the synthetic method. Besides, Sun and Xia maintained that the citrate ions used as capping agent to stabilize the original Ag seeds play a key role in the conversion from spheres into nanoprisms, since they interact preferentially with the {111} facets of the particles, inhibiting their growth.

Other groups have reported the tunability of the Ag nanoprism edge length by adjusting the illumination wavelength. Callegari et al.[23] showed that the photochemical growth of Ag seeds can be controlled through the color of the light used to drive the reaction. They proposed a two-step mechanism based on the initial aggregation of the Ag seeds, which caused the formation of two new populations of larger particles and the subsequent preferential evolution of one of these new species (determined by the illumination conditions) at the expense of the remaining tiny seeds. Bastys et al.[24] used low-intensity light-emitting diodes (LEDs) to photoinduce the formation of Ag nanoprisms from the same Ag seeds, which appeared to be mediated by stages comprising Ostwald ripening or nanoprisms fusion. Again, adjusting the LED emission wavelength, they were able to tune the edge length of the Ag nanoprisms without notably affecting their shape and thickness. Interestingly, this offered the possibility to obtain nanoparticles with strong in-plane surface plasmon resonance bands in the NIR region.

So far, all the methods that we have described are related to the use of light as driving force for the oriented attachment of preformed Ag seeds. Nevertheless, several approaches use light for the photoinduction of the growth of the preformed seeds by the reduction of Ag ions present in the reaction medium. The first report, by Maillard et al.,[25] showed the fabrication of Ag nanoprisms with visible light irradiation for the reduction of silver ions on citrate-stabilized Ag seed surfaces. Again, the final particle size could be tuned by adjusting the illumination wavelength. Recently, it has been demonstrated that irradiation has only impact on the particle size, but minimal effects on their thickness. Furthermore, the origin of particle anisotropy is related to the intrinsic properties of the particles used as seeds rather than to LSPR excitation.

Wet Chemical Reduction by Surfactant-Assisted Methods

Among all available surfactants, cetyltrimethylammonium bromide (CTAB) has become the most extensively used capping agent in the synthesis of Ag and Au nanoparticles. This cationic surfactant has been applied for the preparation of a wide variety of geometries including spheres, rods, or nano- and microplates. In many cases CTAB plays an essential role in acting as shape-directing agent. Generally, these approaches for the preparation of nano- and microplates are based on the reduction of the metal salt with a mild reducing agent, usually ascorbic acid, in the presence of CTAB. For example, by this approach, the synthesis of truncated triangular Ag nanoplates is possible.[26] In this case, CTAB directs the growth of nanoplates through selective adsorption on the (111) plane. The control of plate size, from 40 to 300 nm, was possible by adjusting the concentrations of CTAB and Ag seed.[27] Nevertheless, this method yields particles with a wide size distribution, so that LSPR tuning is rather limited. Seed-mediated approaches, previously developed to produce Au spheres or rods,[28] have also succeeded in preparing Au nanoprisms with average edge lengths of 144 ± 30 nm (Figure 2).[29] Although the procedures for the preparation of spheres, rods, or plates are quite similar to each other, it is believed that surfactant concentration is the critical factor toward producing prisms rather than other shapes. This process involves the successive addition of small Au seeds into three separate growth solutions containing CTAB, Au salt, ascorbic acid, and sodium hydroxide. Although the process also gives rise to a second population of spherical particles (65%), the nanoprisms can be easily separated by using an aluminum oxide filter. Furthermore, the Au nanoprisms can be used as seeds[30] to finely tune their edge length (from ca. 110 to 220 nm) and their optical properties, without altering their original shape or thickness.

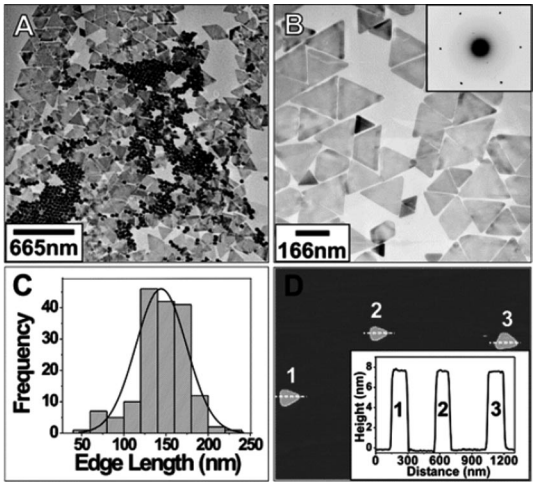

Figure 2. (A) TEM image of Au spherical and triangular nanoparticles. (B) Zoom-in image. The inset shows the electron diffraction pattern of the top of a single prism. (C) Histogram of nanoprism edge lengths. (D) AFM image of nanoprisms on mica (tapping mode). Inset: height profile along the dashed lines. Reproduced with permission from ref.[29]

Other approaches combine the use of CTAB with iodide ions. For example, the addition of traces of iodide to a common synthesis of nanorods is enough to change dramatically the obtained particle morphology to nanoprisms.[31] This effect has been explained on the basis of the preferential adsorption of iodide onto the Au (111) faces, repressing the growth along this direction, and therefore allowing reduction on the other fcc facets. Nevertheless, the formation of spherical particles as byproducts is always observed regardless of iodide concentration. In fact, in a recent work, Fan et al.[32] demonstrated that a key factor to obtain nanoplates, apart from the presence of I^- ions, is the crystalline structure of the seeds. In this method, seeds were prepared

by using sodium citrate as stabilizer, rather than CTAB, leading to particles with stacking faults, which are helpful in obtaining plate-like structures. By adjusting the ratio between Au seeds and I^- ions, it was possible to tune the edge length from 30 to 140 nm, without altering the thickness of the plates. Further investigation of the fundamental aspects of these experimental parameters, together with the use of other reducing agents[33] or temperature,[34] was actually carried out to properly understand and control the fabrication of anisotropic nanomaterials. Thus, we know that temperatures between 50 and 60 °C promote the growth of Au nanoplates. Actually, thermal reduction of $HAuCl_4$ with citrate in the presence of CTAB[35] is one alternative for the preparation of gold plates of variable size, from tens of nanometers to few microns. The proposed growth mechanism[36] for this reaction differs notably from the most widely accepted ones based on the preferential passivation of (111) faces by CTAB adsorption. In this case, it is believed that the formation of nanoplates takes place through the formation of a polycrystalline Au fused mass, which grows in size by incorporating dendritic Au nanostructures and eventually adopting the plate-like morphology.

Another surfactant that is commonly used in the fabrication of nanoplates is bis(2-ethyl-hexyl)sulfosuccinate, AOT. Pileni et al.[37] used reverse micelles of AOT in isooctane to prepare Ag nanodisks by reduction of a silver salt with hydrazine. The size was controlled between 30 and 100 nm by the relative amount of hydrazine. However, the wide size distribution together with the important amount of Ag spheres ruined the interesting optical properties of the nanodisks. Nevertheless, using AOT as stabilizer, Jiang et al.[38] obtained Ag nanoplates and nanodisks with excellent optical properties in the visible-NIR range. They employed a self-seeding co-reduction method comprising a Ag seed suspension with traces of $NaBH_4$, subsequently grown by cooperative reduction with citric and ascorbic acid. Although the reaction products were triangular nanoplates, Ostwald ripening spontaneously promoted the evolution of the plates into disks at room temperature. The same authors discovered that particle evolution could be detained by attaching thiols onto the silver surface.[38b]

Wet Chemical Reduction by Polymer-Assisted Methods

Polyvinylpyrrolidone (PVP) is undoubtedly the most popular polymer in the chemical synthesis of a wide variety of metal nanocrystals since its introduction in the seventies.[39] Although the major role of PVP is to act as capping agent, it has been demonstrated that it may also act as a mild reducing agent.[40] Additionally, PVP has often been claimed to play a key role in determining the final particle morphology, through stronger adsorption onto certain crystalline facets. The first application of PVP to stabilize silver nanoplates (truncated triangles, < 80 nm edge length), was devised by Pastoriza-Santos and Liz-Marzán by using *N*,*N*-dimethylformamide (DMF) as reducing agent and solvent.[8b] A mechanism was proposed involving the aggregation of small Ag nanoparticles, followed by recrystallization into single crystals, so that the edge size could be controlled through the reaction time (at reflux). Also by using DMF as reducing agent, Ag nanoplates were prepared under sonication,[41] which was proposed to assist Ostwald ripening, so that the final morphology was the result of the selective growth of certain crystal planes, guided by PVP. Similar experiments were carried out with ethylene glycol as solvent (the polyol route), also acting as reducing agent at temperatures above 100 °C, which yielded Au microplates with dimensions ranging from several to tens of micrometers in length but only tens to hundreds of nanometers thick.[42] The specific morphology (triangular, truncated triangular, or hexagonal), as well as the size, was found to depend on both temperature and precursor concentration. The presence of large triangular and hexagonal particles with uniform thickness led the authors to propose two main formation mechanisms, one based on the initial growth of small triangular particles, which subsequently grew by Au "atomic attachment" along the <110> direction, and another comprising the connection of the preformed small triangular particles along the (110) lateral planes. Xia et al. also reported different strategies using hydrothermal treatment, also with PVP. An important conclusion from their work[43] was that PVP acts as stabilizer whereas the role of citrate ions is directly related to inducing the final shape. The same group later showed the possibility of synthesizing Ag nanoplates, following also a hydrothermal process in the presence of PVP.[44] Importantly, PVP not only protected the particles from aggregation but also acted as the reducing agent. A mechanism to explain particle formation based on the addition of Ag atoms onto trimeric silver clusters was also proposed.[45] This method allowed tuning the nanoplate lateral dimensions between 50 and 350 nm while keeping the thickness constant (ca. 5 nm) so that their optical properties could be tailored within the whole stretch of the visible and NIR regions. Hydrothermal synthesis of Au plates was also reported with PVP,[44] but the obtained plates were in the micrometer scale, rather polydisperse both in size and shape, and in relatively low yield. Exception can be made of the work of Ah et al.,[46] who reported the hydrothermal synthesis of Au nanoplates in high yield, using citrate and PVP, with control over edge length (80–500 nm) and width (10–40 nm) by simply adjusting the molar ratio between the citrate/PVP mixture and the Au salt (Figure 3). Since the mechanism proposed was based on a seeding growth process, the relative amount of nuclei with respect to the remaining Au salt would determine the final nanoplate size. The tight control and monodispersity of the nanoplates was reflected in the excellent optical properties with an in-plane dipolar surface plasmon resonance band tunable from 700 to 2000 nm. In another interesting report, in which PVP was claimed to act as reducing agent, Zhang et al.[47] used a ternary system constituted by water, PVP, and *n*-pentyl alcohol to synthesize Ag nanoprisms with tunable edge lengths from 24 to 120 nm by just changing the amount of PVP. Consequently, the main surface plasmon band was also tuned from 475 nm to

891 nm. The authors proposed an intricate growth mechanism based on the initial formation of a (water/water-PVP)$_n$/*n*-pentyl alcohol (WWPN) interface region where the Ag^+ ions diffused and were reduced. Since the selective adsorption of PVP on specific crystallographic planes of Ag occurred, further reduction of silver ions took place preferentially on those crystallographic planes with hindered PVP adsorption, inducing the formation of nanoprisms.

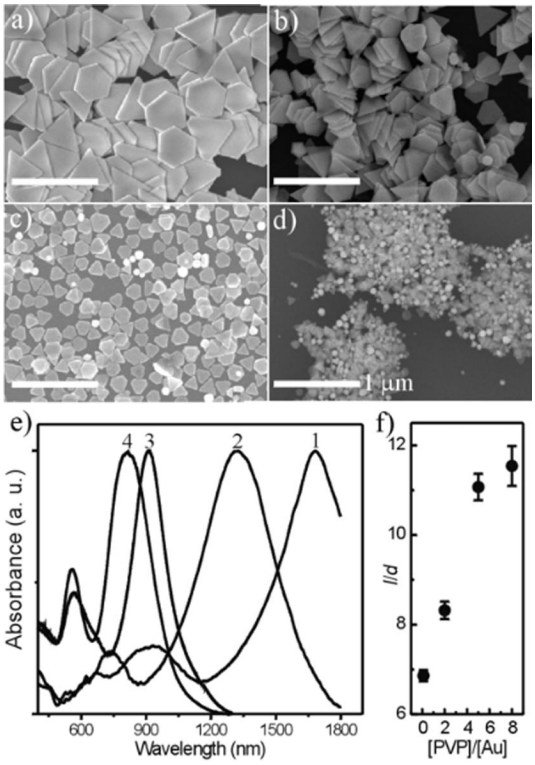

Figure 3. (a–d) FE-SEM images of gold nanoplates with average width and thickness of 450 ± 29 and 39 ± 4 nm (a), 310 ± 25 and 28 ± 3 nm (b), 158 ± 13 and 18 ± 3 nm (c), and 96 ± 12 and 14 ± 2 nm (d), respectively. The molar ratio of the repeating unit of PVP (MW = 55 000, *n* = 500) to $HAuCl_4$ was 8:1 (a), 5:1 (b), 2:1 (c), and 0.1:1 (d). The scale bar is 1 μm. (e) UV/Vis/NIR extinction spectra of the samples in panels (a–d). Spectra 1–4 were obtained from the corresponding samples a–d. The solutions of larger gold nanoplates were suspended in D_2O for the measurement to avoid absorption due to H_2O. (f) Aspect ratio (width/thickness) as a function of the molar ratio of PVP to Au. Reproduced with permission from ref.[46]

Finally, it is worth noting that conversion of Ag nanoparticles in the dark, but in the presence of $NaBH_4$, H_2O_2, PVP, and citrate, has been used for a fine control over plate thickness from 4 to 7 nm. While $NaBH_4$ was the critical factor affecting the conversion of silver nanoparticles into nanoprisms, and thereby controlling edge length, thickness, and even tip sharpness, PVP and citrate acted as stabilizer and shape-guiding agent, respectively.

Other Wet Chemical Reduction Methods

As demonstrated by Gentry et al.,[48] hydroquinone (HQ), in the presence of tiny Ag seeds, is a suitable reducing agent to obtain not only Ag spherical particles but also nanoprisms (<100 nm in edge length). In the case of nanoprisms, the final morphology, that is triangular, truncated triangular, hexagonal, or even circular, depended on the experimental conditions. The key factor was the capping agent, more controlled and monodisperse nanoprisms being obtained when citrate was used, whereas PVP or poly(vinyl alcohol) (PVA) led to higher polydispersity. Other parameters that need to be taken into account are pH (which modifies the reducing character of HQ) and HQ concentration. It seems that the LSPR position can be tuned from approximately 1000 nm to 500 nm by playing with the experimental conditions (including reaction time), but the characterization of the particle dimensions was not sufficiently accurate. The proposed mechanism was based on random crystal growth into the final morphology, rather than formation of small nanoprisms by seed aggregation/melting. Conversely, a PVA film was used for the in situ synthesis of polygonal Au nanoplates through thermal treatment, in which the polymer acted as reducing agent and stabilizer (Figure 4).[49] Adjusting the Au/PVA ratio, time, and temperature of fabrication, the authors were able to tune the morphology of the polygonal nanoplates.

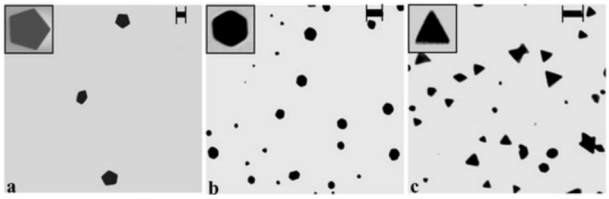

Figure 4. TEM images of Au-PVA films with polygonal nanoplates generated under different conditions. The Au/PVA ratio, temperature of heating (°C), and time of heating (min) are indicated in that order in parentheses: (a) pentagons (0.04, 170, 5); (b) hexagons (0.08, 130, 30); (c) triangles (0.12, 100, 60). Scale bar: 50 nm. The insets show enlarged views of a single nanoplate with the dominant shape in each case. Reproduced with permission from ref.[49]

Block copolymers were also used to synthesize Au nano- and microplates. Lee et al.[50] fabricated large Au microplates by thermal reduction by using Pluronic P123 as both reducing and capping agent. By using a similar strategy but with an amphiphilic triblock copolymer made of polyethylene oxide and polystyrene oxide, Au nanoplates were obtained with optical response in the NIR region. Temperature was a key factor in the final particle morphology, yielding triangular and hexagonal plates in high yield (ca. 70%) at 65 °C. Particle size could also be tuned from approximately 100 to 1000 nm by adjusting the copolymer-to-gold-salt ratio and aging time.

Wet Chemical Reduction by Biomolecule-Assisted Methods

The utilization of natural moieties (microorganisms, plant extracts, and soil) has recently emerged as an interesting strategy for the synthesis of biocompatible metal nanoparticles. Focusing on nanoplates, the first reported synthe-

sis of Au nanoplates in high quantities by using a natural product yielded a mix of truncated and nontruncated single-crystalline triangles with a wide size distribution (from 50 to 1500 nm). This method was based on a single-step reduction of gold hydrochloride by using lemongrass extract as reducing and shape-directing agent.[51] Although a large amount of Au spheres was also produced (55%), these were easily removed by centrifugation. The optical features of the purified samples were those typical for Au nanoplates, and the main plasmon resonance band was located in the NIR region. While the particle size could be tuned by changing the amount of lemongrass leaf extract,[52] the morphology was found also to be affected by halide ions and temperature.[53] Following a similar approach but using *Aloe vera* extract, the same group synthesized Au nanotriangles with interesting optical properties in the NIR region.[54] Lee et al.[55] also investigated the synthesis of Au and Ag nanoplates by using natural products. For example, gold salt can be reduced to nanoparticles with *Sargassum sp.* extract. The optimal growth of single-crystalline Au nanoplates in high yield (ca 80–90%) was achieved by working at neutral pH and room temperature. By varying the initial reactant concentrations, it was possible to tune the edge length of the nanoplates in the range 200–800 nm.[55a] In follow-up studies,[55b,55c] the use of the extract of the unicellular alga *Chlorella vulgaris* allowed the identification of a protein with approximately 28 kDa that was the major biomolecule involved in the synthesis of Au nanoplates. Gold reduction was achieved mainly by the Tyr residues, while the carboxylic groups acted as shape-directing agents. Thus, when the isolated protein was used, micron-sized triangular and hexagonal nanoplates were obtained in high yield (90%). Although the protein concentration can tune the product size from micrometer to nanometer scale, it also affects the yield. Finally, the use of peptides has also been reported for nanoplates synthesis. Zhang et al.[56] used glycyl glycine as reducing, capping, and shape-directing agent in a hydrothermal process that resulted in Ag nanoplates larger than 100 nm. Finally, Tan et al.[57] synthesized in situ Au nanoplates within a multilayer thin film based on an assembly of a polypeptide (polyaspartic acid, pLAA) and polyethyleneimide (LPEI). In this case, pLAA acts as reducing agent (through the carboxyl side groups) for the Au salt. It was claimed that the reduction rate could be enhanced by increasing the α-helix content of pLAA, which increased with the number of bilayers in the film and therefore allowed lateral size control within a small range (20–60 nm).

Lithography Methods

An alternative to the wet chemical and photoinduced methods is provided by lithography techniques. While electron-beam lithography has been successfully employed in the patterning of arrayed plates over large areas,[58] it is extremely time consuming. Nevertheless, large-scale production of surface-bound triangular nanoparticle arrays can be achieved though nanosphere lithography (NSL). This multistep strategy, mainly developed by Van Duyne et al.,[59] has been demonstrated to be suitable for tuning particle sizes between 20 and 1000 nm and can be applied to Ag, Au, and other materials, with a good control over the shape and interparticle spacing. The conventional NSL process begins with self-assembly of colloidal (typically polystyrene or silica) nanospheres onto a substrate, which are then used as a mask during the physical evaporation of the desired material(s), followed by removal of the mask by sonication. Whereas the nanosphere diameters determine the final size and interparticle distance, the shape is ultimately controlled by the precision of the template, the metal evaporation angle,[59f,60] or even by post-deposition processes, such as sintering.[59e] Thus, if the substrate is positioned normal to the direction of material deposition, triangular nanoplates are obtained (Figure 5). Although initially the typical size of defect-free domains was in the 10–100 μm^2 range, several authors have been able to fabricate large-area (up to 1 cm^2) Ag nanoparticle arrays by exploiting convective self-assembly for mask preparation.[59d] Van Duyne et al. have also demonstrated the possibility of releasing into solution Ag nanoprisms prepared by NSL,[59a] through functionalization of the particles with thiolated molecules prior to their release, to prevent aggregation. However, as the release is induced by sonication, some particles may break up during this process, thus limiting further application.

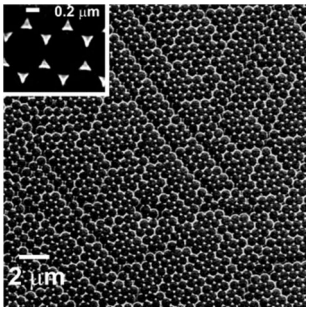

Figure 5. SEM images of Ag nanoparticle arrays on indium tin oxide (ITO). The nanosphere diameter was 590 nm, and the mass thickness of the silver film was 67 nm. Reproduced with permission from ref.[59e]

Optical Enhancing Properties of Noble Metal Nanoplates

Prior to the development of efficient synthetic methods for the fabrication of triangular nano- and microprisms, the theoretical description of the plasmonic response of metal nanoparticles was basically restricted to objects with spherical symmetry, including spheres and ellipsoids, on the basis of analytical methods (Mie–Gans theory). However, it was not possible to apply such simplification for the resolution of Maxwell's equations to objects with lower symmetry (high anisotropy), such as plates, and therefore numerical

methods were required. The first combined report in which experimental spectra were compared to numerical simulations was published in 2001, for the light-induced aggregation method.[18] In this paper, the discrete dipole approximation (DDA)[61] was used for resolving Maxwell's equations, and it was possible not only to find a good correlation with the experimental spectra, but also to propose an assignment of the different plasmon modes, in terms of in-plane and out-of-plane dipolar and quadrupolar resonances. These calculations thus revealed a complex plasmonic response due to the anisotropy of the particles. Although the precise energy of the different modes is strongly dependent on the specific dimensions of the plates, the authors also needed to include truncation effects in order to find a good agreement with their observations. Further advances in the preparation methods allowed several authors to compare their experimental spectra with simulations, but even when dilute colloids were used, small polydispersity inevitably led to broadening and loss of accuracy because of averaging effects. To overcome this limitation, single-particle studies have been implemented for the analysis of metal nanoparticle plasmonic properties. By using an optical microscope with a dark-field condenser, Van Duyne and co-workers[62] recorded resonant Rayleigh scattering spectra from single silver nanoprisms, which indeed resulted in much narrower bands than those for the corresponding ensemble spectrum. Additionally, Van Duyne et al. showed that changes in solvent refractive index or adsorption of alkanethiols resulted in significant LSPR shifts, which opened the way toward application of such nanoprisms as LSPR biosensing substrates. A latter work by Mulvaney and colleagues[63] showed similar results with gold triangular prisms, which offer the advantage of higher chemical stability. However, dark-field optical microspectroscopy still poses certain limitations in spatial resolution, so that it cannot provide direct evidence of the electric field enhancement intensity and distribution within the nanoparticles, which is extremely important for many plasmonic applications. With the increased resolution of electron energy detectors in scanning transmission electron microscopy (STEM), the possibility of mapping the different surface plasmon resonance modes within a single nanoparticle has become possible through electron energy loss spectroscopy (EELS). One of the first reports[11b] dealing with such characterization showed that, as theoretically predicted,[64] the plasmonic response of a silver nanotriangle comprised three main contributions with maximum electromagnetic field enhancement (or energy loss) localized at the center, the edges, or the corners of the triangle. These experimental results were perfectly reproduced and explained by using the boundary element method (BEM), an alternative numerical method for the resolution of Maxwell's equations, applied to the calculation of EELS distributions. In a recent expanded report by the same authors,[11a] the plasmon distribution was analyzed in triangles with different dimensions, from 70 to 300 nm edge length (Figure 6), invariably containing the three main plasmonic contributions but red-shifted as the side length was increased. Furthermore, the EEL intensity also increased with particle size, which can be correlated with the efficiency of a given nanostructure for optical field enhancement.

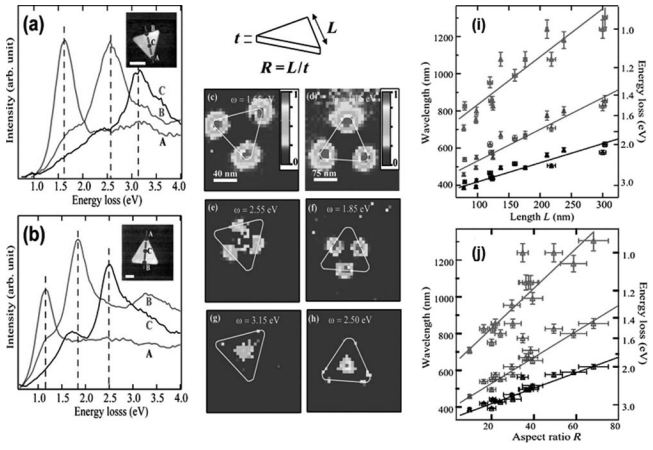

Figure 6. Size-dependent mapping of plasmons in silver nanoprisms. EELS spectra acquired at a corner (A), the middle point of an edge (B), and the center (C) of nanoprisms with an edge length of 97 nm (thickness 4 nm) (a) and 176 nm (thickness 6 nm) (b). The corresponding insets show the HAADF images of each nanoprism and the exact positions at which the EEL data were measured. In each case, three main resonances were identified. The energies of these modes vary from one prism to another. Panels c, e, and g present maps of the intensity distributions of the main resonances detected on the prism in (a). Similarly, panels d, f, and h show the intensity maps of the three modes on the prism in (b). For each set of three maps, the common intensity scale is linear and is expressed in arbitrary units. The general inset of this figure defines the two dimensions t and L. Energy dependence of the surface plasmons of silver nanoprisms on (i) the edge length L and (j) the aspect ratio $R = L/t$, as deduced from experimental images. Top: corner mode; middle: edge mode; bottom: center mode. Reproduced with permission from ref.[11a]

Although the complete understanding of the plasmon modes in nanoplates is very recent, they have been widely applied as optical enhancers for surface-enhanced Raman scattering (SERS) during the last decade. For example, one of the first reports[65] on gold and silver nanoplates as SERS substrates demonstrated the comparable performance of these structures with conventional gold and silver citrate reduced colloidal suspensions, the most common platforms for SERS. These seminal results were obtained in suspension by average SERS, that is, SERS from an ensemble of colloidal particles and aggregates, and characterized by a stable average spectrum with well-defined frequency and bandwidth.[15a] The characteristic features of this experiment, in which the analyte is naturally adsorbed in solution and the particles present in the sample volume are constantly renewed as a result of Brownian motion, together with the intrinsic contamination with other plasmonic structures in the sample (mainly spheres), did not allow the realization of the full potential of nanoplates as optical enhancing platforms. In fact, although it has been demonstrated that triangles and plates provide higher signals in average SERS for the detection of various analytes including organic pollutants, inorganic anions, or biomolecules,[66] their complete optical performance is still hindered

by several factors. First of all, the synthetic routes usually include the use of polymers, such as PVP or small molecules like CTAB or thiols, which strongly bind onto the nanoparticle surface.[67] The net effect is a partial (or even complete) passivation of the metallic surfaces to adsorb the target molecule, so that small or zero optical enhancement is achieved. Second, even when dealing with easily exchangeable capping agents as citrate or porous polymers, such as polyvinyl alcohol (PVA) or polystyrene sulfonate (PSS), which would permit adsorption, in particular for thiolated or aminated molecules, the adsorption of the analyte cannot be directed toward the "hot" areas within the nanoplate, but it is rather adsorbed on the whole metal surface. This statistical adsorption severely limits the efficiency derived from the high concentration of the electric field at sharp tips.[68] Thus, strategies to gain advantage from nanoparticle morphology by using clean surfaces have been developed. We have described above a useful alternative that can help solve this problem, namely the use of nanosphere lithography (NSL).[59] These substrates can be easily produced over areas larger than 1 cm^2 (Figure 5), and their optical properties can be tuned within the visible and the NIR range by changing either the size of the templating polystyrene spheres and/or by augmenting the evaporation time of the metal.[69] Additionally, the gap distance between two sharp tips can be adjusted to obtain highly active hot spots (i.e. spatial regions between two or more plasmonic nanostructures where the electromagnetic field is extremely high due to plasmon coupling).[16a,70] These substrates have been demonstrated to function as quantitative ultrasensitive platforms, and they have been applied to a number of interesting biological problems, such as ultradetection of anthrax spores,[71] in vivo detection of lactate,[72] or real-time in vivo detection of glucose.[73] Still, the success of NSL as SERS substrate is compromised because it is not possible to take full advantage of the extraordinary optical properties of the nanoplates as the analyte can still be retained on the whole available surface. While other alternatives to optimize the mass production of patterned platforms are being developed, such as, for example, colloidal stamping,[74] nowadays the most promising way of taking full benefit of plasmonic nanoplates involves the use of single particles as SERS sensing elements.

Conclusions

The synthesis of noble metal nanoplates (gold and silver in particular) has been greatly advanced during the last decade, especially by making use of colloid chemistry methods, so that basically "pure" colloids can be obtained, with the potential of tailoring the average particle size through synthesis parameters. However, the understanding of the precise growth mechanisms is still rather poor, and further work in this area is required. The high level of control over nanoplate dimensions in turn permits tuning the optical response within the visible and the NIR areas of the electromagnetic spectrum. Although the characterization and understanding of such optical response has advanced to unsuspected limits, actual exploitation of the efficient plasmonic response still requires a further degree of handling and directed assembly, so that, for example, analyte molecules can be directed toward the "hot areas", where electromagnetic field acquires very high values.[75]

Acknowledgments

R. A. A.-P. acknowledges the RyC (MiCInn, Spain) program. This work has been funded by the Spanish Ministerio de Ciencia e Innovación/FEDER (Grants MAT2007-62696 and MAT2008-05755), Consolider Ingenio (Grant2010-CSD2006-12), and the Xunta de Galicia (Grants PGIDIT06TMT31402PR and 08TMT008314PR).

[1] a) M. Pelton, J. Aizpurua, G. Bryant, *Laser Photon. Rev.* **2008**, *2*, 136–159; b) F. J. García de Abajo, *Rev. Mod. Phys.* **2007**, *79*, 1267.
[2] J. A. Schuller, E. S. Barnard, W. S. Cai, Y. C. Jun, J. S. White, M. L. Brongersma, *Nat. Mater.* **2010**, *9*, 193–204.
[3] H. A. Atwater, A. Polman, *Nat. Mater.* **2010**, *9*, 205–213.
[4] a) M. Sanles-Sobrido, M. A. Correa-Duarte, S. Carregal-Romero, B. Rodriguez-Gonzalez, R. A. Alvarez-Puebla, P. Herves, L. M. Liz-Marzan, *Chem. Mater.* **2009**, *21*, 1531–1535; b) J. R. Adleman, D. A. Boyd, D. G. Goodwin, D. Psaltis, *Nano Lett.* **2009**, *9*, 4417–4423.
[5] a) B. Sepulveda, P. C. Angelome, L. M. Lechuga, L. M. Liz-Marzan, *Nano Today* **2009**, *4*, 244–251; b) K. A. Willets, R. P. Van Duyne, *Ann. Rev. Phys. Chem.* **2007**, *58*, 267–297; c) R. A. Alvarez-Puebla, L. M. Liz-Marzan, *Small* **2010**, *6*, 604–610.
[6] a) E. Boisselier, D. Astruc, *Chem. Soc. Rev.* **2009**, *38*, 1759–1782; b) X. Huang, S. Neretina, M. A. El-Sayed, *Adv. Mater.* **2009**, *21*, 4880–4910; c) K. Riehemann, S. W. Schneider, T. A. Luger, B. Godin, M. Ferrari, H. Fuchs, *Angew. Chem. Int. Ed.* **2009**, *48*, 872–897; d) P. K. Jain, X. H. Huang, I. H. El-Sayed, M. A. El-Sayed, *Acc. Chem. Res.* **2008**, *41*, 1578–1586.
[7] a) X. Lu, M. Rycenga, S. E. Skrabalak, B. Wiley, Y. Xia, *Ann. Rev. Phys. Chem.* **2009**, *60*, 167–192; b) C. J. Murphy, T. K. Sau, A. M. Gole, C. J. Orendorff, J. Gao, L. Gou, S. E. Hunyadi, T. Li, *J. Phys. Chem. B* **2005**, *109*, 13857–13870; c) T. K. Sau, C. J. Murphy, *J. Am. Chem. Soc.* **2004**, *126*, 8648–8649; d) C. Burda, X. Chen, R. Narayanan, M. A. El-Sayed, *Chem. Rev.* **2005**, *105*, 1025–1102.
[8] a) I. Pastoriza-Santos, L. M. Liz-Marzan, *J. Mater. Chem.* **2008**, *18*, 1724–1737; b) I. Pastoriza-Santos, L. M. Liz-Marzán, *Nano Lett.* **2002**, *2*, 903–905.
[9] a) J. Zhao, A. O. Pinchuk, J. M. McMahon, S. Z. Li, L. K. Ausman, A. L. Atkinson, G. C. Schatz, *Acc. Chem. Res.* **2008**, *41*, 1710–1720; b) V. Myroshnychenko, J. Rodriguez-Fernandez, I. Pastoriza-Santos, A. M. Funston, C. Novo, P. Mulvaney, L. M. Liz-Marzan, F. J. Garcia de Abajo, *Chem. Soc. Rev.* **2008**, *37*, 1792–1805.
[10] J. Rodriguez-Fernandez, C. Novo, V. Myroshnychenko, A. M. Funston, A. Sanchez-Iglesias, I. Pastoriza-Santos, J. Perez-Juste, F. J. Garcia de Abajo, L. M. Liz-Marzan, P. Mulvaney, *J. Phys. Chem. C* **2009**, *113*, 18623–18631.
[11] a) J. Nelayah, M. Kociak, O. Stéphan, N. Geuquet, L. Henrard, F. J. De García Abajo, I. Pastoriza-Santos, L. M. Liz-Marzán, C. Colliex, *Nano Lett.* **2010**, *10*, 902–907; b) J. Nelayah, M. Kociak, O. Stéphan, F. J. Garcia de Abajo, M. Tencé, L. Henrard, D. Taverna, I. Pastoriza-Santos, L. M. Liz-Marzán, C. Colliex, *Nature Phys.* **2007**, *3*, 348–353.
[12] a) M. Kuttge, E. J. R. Vesseur, A. F. Koenderink, H. J. Lezec, H. A. Atwater, F. J. Garcia de Abajo, A. Polman, *Phys. Rev. B* **2009**, 79–85; b) G. W. Bryant, F. J. García de Abajo, J. Aizpurua, *Nano Lett.* **2008**, *8*, 631–636.

[13] a) P. S. Kumar, I. Pastoriza-Santos, B. Rodriguez-Gonzalez, F. J. Garcia de Abajo, L. M. Liz-Marzan, *Nanotechnology* **2008**, 19–26; b) L. Rodriguez-Lorenzo, R. A. Alvarez-Puebla, I. Pastoriza-Santos, S. Mazzucco, O. Stephan, M. Kociak, L. M. Liz-Marzan, F. J. Garcia de Abajo, *J. Am. Chem. Soc.* **2009**, *131*, 4616–4618.
[14] N. Pazos-Perez, S. Barbosa, L. Rodriguez-Lorenzo, P. Aldeanueva-Potel, J. Perez-Juste, I. Pastoriza-Santos, R. A. Alvarez-Puebla, L. M. Liz-Marzan, *J. Phys. Chem. Lett.* **2010**, *1*, 24–27.
[15] a) R. F. Aroca, R. A. Alvarez-Puebla, N. Pieczonka, S. Sanchez-Cortez, J. V. Garcia-Ramos, *Adv. Colloid Interface Sci.* **2005**, *116*, 45–61; b) R. A. Alvarez-Puebla, R. F. Aroca, *Anal. Chem.* **2009**, *81*, 2280–2285.
[16] a) L. Brus, *Acc. Chem. Res.* **2008**, *41*, 1742–1749; b) J. R. Lombardi, R. L. Birke, *Acc. Chem. Res.* **2009**, *42*, 734–742.
[17] J. Zhu, Y. Shen, A. Xie, L. Qiu, Q. Zhang, Z. Zhang, *J. Phys. Chem. C* **2007**, *111*, 7629–7633.
[18] R. Jing, Y. W. Cao, C. A. Mirkin, K. L. Kelly, G. C. Schatz, J. G. Zheng, *Science* **2001**, *294*, 1901–1903.
[19] R. Jing, Y. W. Cao, E. Hao, G. S. Métraux, G. C. Schatz, C. A. Mirkin, *Nature* **2003**, *425*, 487–490.
[20] C. Xue, C. A. Mirkin, *Angew. Chem. Int. Ed.* **2007**, *46*, 2036–2038.
[21] A. M. Junior, H. P. M. de Oliveira, M. H. Gehlen, *Photochem. Photobiol. Sci.* **2003**, *2*, 921–925.
[22] Y. Sun, Y. Xia, *Adv. Mater.* **2003**, *15*, 695–699.
[23] A. Callegari, D. Tonti, M. Chergui, *Nano Lett.* **2003**, *3*, 1565–1568.
[24] V. Bastys, I. Pastoriza-Santos, B. Rodríguez-González, R. Vaisnoras, L. M. Liz-Marzán, *Adv. Funct. Mater.* **2006**, *16*, 766–773.
[25] M. Maillard, P. Huang, L. Brus, *Nano Lett.* **2003**, *3*, 1611–1615.
[26] a) S. Chen, D. L. Carroll, *Nano Lett.* **2002**, *2*, 1003–1007; b) S. Chen, Z. Fan, D. L. Carroll, *J. Phys. Chem. B* **2002**, *106*, 10777–10781.
[27] S. Chen, D. L. Carroll, *J. Phys. Chem. B* **2004**, *108*, 5500–5506.
[28] N. Jana, l. Gearheart, C. J. Murphy, *Chem. Mater.* **2001**, *13*, 2313–2322.
[29] J. E. Millstone, S. Park, K. L. Shuford, L. Qin, G. C. Schatz, C. A. Mirkin, *J. Am. Chem. Soc.* **2005**, *127*, 5312–5313.
[30] J. E. Millstone, G. S. Métraux, C. A. Mirkin, *Adv. Funct. Mater.* **2006**, *16*, 1209–1214.
[31] T. H. Ha, H. J. Koo, B. H. Chung, *J. Phys. Chem. C* **2007**, *111*, 1123.
[32] X. Fan, Z. Guo, J. Hong, Y. Zhang, J. N. Zhang, N. Gu, *Nanotechnology* **2010**, *21*, 105602.
[33] L. Zhang, C. Z. Huang, Y. F. Li, Q. Li, *Cryst. Growth Des.* **2009**, *9*, 3211–3217.
[34] H. M. Chen, R.-S. Liu, D. P. Tsai, *Cryst. Growth Des.* **2009**, *9*, 2079–2087.
[35] H.-C. Chu, C.-H. Kuo, M. H. Huang, *Inorg. Chem.* **2006**, *45*, 808–813.
[36] W. L. Huang, C. C. Chen, M. H. Huang, *J. Phys. Chem. C* **2007**, *111*, 2533–2538.
[37] a) M. Maillard, S. Giorgio, M.-P. Pileni, *Adv. Mater.* **2002**, *14*, 1084; b) M. Maillard, S. Giorgio, M.-P. Pileni, *J. Phys. Chem. B* **2003**, *107*, 2466–2470.
[38] a) X. Jiang, Q. Zheng, A. Yu, *Nanotechnology* **2006**, *17*, 4929–4935; b) X. Jiang, Q. Zheng, A. Yu, *Langmuir* **2007**, *23*, 2218–2223.
[39] H. Hirai, Y. Nakao, N. Toshima, *Chem. Lett.* **1978**, 545–548.
[40] I. Washio, Y. Xiong, Y. Yin, Y. Xia, *Adv. Mater.* **2006**, *18*, 1745–1749.
[41] L.-P. Jiang, S. Xu, J.-M. Zhu, J.-R. Zhang, J.-J. Zhu, H.-Y. Chen, *Inorg. Chem.* **2004**, *43*, 5877–5883.
[42] C. Li, W. Cai, B. Cao, F. Sun, Y. Li, C. Kan, L. Zhang, *Adv. Funct. Mater.* **2006**, *16*, 83–90.
[43] Y. Sun, B. Mayers, Y. Xia, *Nano Lett.* **2003**, *3*, 675–679.
[44] Y. Xiong, I. Washio, J. Chen, H. Cai, Z.-Y. Li, Y. Xia, *Langmuir* **2006**, *22*, 8563–8570.
[45] Y. Xiong, I. Washio, J. Chen, M. Sadilek, Y. Xia, *Angew. Chem. Int. Ed.* **2007**, *46*, 4917–4921.
[46] C. S. Ah, Y. J. Yun, H. J. Park, W. J. Kim, D. H. Ha, W. S. Yun, *Chem. Mater.* **2005**, *17*, 5558–5561.
[47] J. Zhang, H. Liu, P. Zhan, Z. Wang, N. Ming, *Adv. Funct. Mater.* **2007**, *17*, 1558–1566.
[48] a) S. T. Gentry, S. J. Fredericks, R. Krchnavek, *Langmuir* **2009**, *25*, 2613–2621; b) S. T. Gentry, S. D. Levit, *J. Phys. Chem. C* **2009**, *113*, 12007–12015.
[49] S. Porel, S. Singh, T. P. Radhakrishnan, *Chem. Commun.* **2005**, 2387–2389.
[50] a) J. U. Kim, S. H. Cha, K. Shin, J. Y. Jho, J. C. Lee, *Adv. Mater.* **2004**, *16*, 459–464; b) W.-K. Lee, S.-H. Cha, K.-H. Kim, B.-W. Kim, J.-C. Lee, *J. Solid State Chem.* **2009**, *182*, 3243–3248.
[51] S. S. Shankar, A. Rai, B. Ankamwar, A. Singh, A. Ahmad, M. Sastry, *Nat. Mater.* **2004**, *3*, 482–488.
[52] S. S. Shankar, A. Rai, A. Ahmad, M. Sastry, *Chem. Mater.* **2005**, *17*, 566–572.
[53] A. Rai, A. Singh, A. Ahmad, M. Sastry, *Langmuir* **2006**, *22*, 736–741.
[54] S. P. Chandran, M. Chaudhary, R. Pasricha, A. Ahmad, M. Sastry, *Biotechnol. Prog.* **2006**, *22*, 577–583.
[55] a) B. Liu, J. Xie, J. Y. Lee, Y. P. Ting, J. P. Chen, *J. Phys. Chem. B* **2005**, *109*, 15256–15263; b) J. Xie, J. Y. Lee, D. I. Wang, Y. P. Ting, *ACS Nano* **2007**, *1*, 429–439; c) J. Xie, J. Y. Lee, D. I. C. Wang, Y. P. Ting, *Small* **2007**, *3*, 672–682.
[56] J. Yang, L. Lu, H. Wang, W. Shi, H. Zhang, *Cryst. Growth Des.* **2006**, *6*, 2155–2158.
[57] Y. N. Tan, J. Y. Lee, D. I. C. Wang, *J. Phys. Chem. C* **2009**, *113*, 10887–10895.
[58] a) N. A. Abu Hatab, J. M. Oran, M. J. Sepaniak, *ACS Nano* **2008**, *2*, 377–385; b) D. P. Fromm, A. Sundaramurthy, P. J. Schuck, G. Kino, W. E. Moerner, *Nano Lett.* **2004**, *4*, 957–961.
[59] a) A. J. Haes, J. Zhao, S. Zou, C. S. Own, L. D. Marks, G. C. Schatz, R. P. Van Duyne, *J. Phys. Chem. B* **2005**, *109*, 11158–11162; b) C. L. Haynes, R. P. Van Duyne, *J. Phys. Chem. B* **2001**, *105*, 5599–5611; c) J. C. Hulteen, R. P. Van Duyne, *J. Vac. Sci. Technol. A* **1995**, *13*, 1553–1558; d) A. D. Ormonde, E. C. M. Hicks, J. Castillo, R. P. Van Duyne, *Langmuir* **2004**, *20*, 6927–6931; e) X. Zhang, E. M. Hicks, J. Zhao, G. C. Schatz, R. P. Van Duyne, *Nano Lett.* **2005**, *5*, 1503–1507; f) C. L. Haynes, R. P. Van Duyne, *Nano Lett.* **2003**, *3*, 939–942.
[60] M. C. Gwinner, E. Koroknay, L. Fu, P. Patoka, W. Kandulski, M. Giersig, H. Giessen, *Small* **2009**, *5*, 400–406.
[61] K. L. Kelly, E. Coronado, L. L. Zhao, G. C. Schatz, *J. Phys. Chem. B* **2003**, *107*, 668–677.
[62] L. J. Sherry, R. Jin, C. A. Mirkin, G. C. Schatz, R. P. Van Duyne, *Nano Lett.* **2006**, *6*, 2060–2065.
[63] C. Novo, A. M. Funston, I. Pastoriza-Santos, L. M. Liz-Marzán, P. Mulvaney, *J. Phys. Chem. C* **2008**, *112*, 3–7.
[64] C. L. Haynes, A. D. McFarland, L. Zhao, R. P. Van Duyne, G. C. Schatz, L. Gunnarsson, J. Prikulis, B. Kasemo, M. Kall, *J. Phys. Chem. B* **2003**, *107*, 7337–7342.
[65] I. Lee, S. W. Han, K. Kim, *J. Raman Spectrosc.* **2001**, *32*, 947–952.
[66] a) Y. Sun, G. P. Wiederrecht, *Small* **2007**, *3*, 1964–1975; b) R. Baigorri, J. M. García-Mina, R. F. Aroca, R. A. Alvarez-Puebla, *Chem. Mater.* **2008**, *20*, 1516–1521; c) D. S. Dos Santos Jr., R. A. Alvarez-Puebla, O. N. Oliveira Jr., R. F. Aroca, *J. Mater. Chem.* **2005**, *15*, 3045–3049; d) R. A. Alvarez-Puebla, D. S. Santos Jr., R. F. Aroca, *Analyst* **2007**, *132*, 1210–1214; e) X. C. Jiang, A. B. Yu, *Langmuir* **2008**, *24*, 4300–4309.
[67] J. Zhang, Y. Gao, R. A. Alvarez-Puebla, J. M. Buriak, H. Fenniri, *Adv. Mater.* **2006**, *18*, 3233–3237.
[68] L. Rodriguez-Lorenzo, R. A. Alvarez-Puebla, F. J. Garcia de Abajo, L. M. Liz-Marzan, *J. Phys. Chem. C* **2010**, *114*, 7336–7340.

[69] a) C. L. Haynes, R. P. Van Duyne, *J. Phys. Chem. B* **2003**, *107*, 7426–7433; b) J. P. Camden, J. A. Dieringer, J. Zhao, R. P. Van Duyne, *Acc. Chem. Res.* **2008**, *41*, 1653–1661.
[70] S. J. Lee, Z. Guan, H. Xu, M. Moskovits, *J. Phys. Chem. C* **2007**, *111*, 17985–17988.
[71] X. Zhang, M. A. Young, O. Lyandres, R. P. Van Duyne, *J. Am. Chem. Soc.* **2005**, *127*, 4484–4489.
[72] N. C. Shah, O. Lyandres, J. T. Walsh, M. R. Glucksberg, R. P. Van Duyne, *Anal. Chem.* **2007**, *79*, 6927–6932.
[73] a) O. Lyandres, N. C. Shah, C. R. Yonzon, J. T. Walsh, M. R. Glucksberg, R. P. Van Duyne, *Anal. Chem.* **2005**, *77*, 6134–6139; b) D. A. Stuart, J. M. Yuen, N. Shah, O. Lyandres, C. R. Yonzon, M. R. Glucksberg, J. T. Walsh, R. P. Van Duyne, *Anal. Chem.* **2006**, *78*, 7211–7215.
[74] N. Pazos-Pérez, W. Ni, A. Schweikarta, R. A. Alvarez-Puebla, A. Fery, L. M. Liz-Marzán, *Chemical Science* **2010**, DOI: 10.1039/c0sc00132e.
[75] a) W. Li, P. H. C. Camargo, L. Au, Q. Zhang, M. Rycenga, Y. Xia, *Angew. Chem. Int. Ed.* **2010**, *49*, 164–168; b) M. Rycenga, P. H. C. Camargo, W. Li, C. H. Moran, Y. Xia, *J. Phys. Chem. Lett.* **2010**, *1*, 696–703.

Received: May 23, 2010
Published Online: July 9, 2010

